Spata6 is required for normal assembly of the sperm connecting piece and tight head–tail conjunction

Shuiqiao Yuan[a], Clifford J. Stratton[a], Jianqiang Bao[a], Huili Zheng[a], Bhupal P. Bhetwal[a], Ryuzo Yanagimachi[b,1], and Wei Yan[a,c,1]

[a]Department of Physiology and Cell Biology, University of Nevada School of Medicine, Reno, NV 89557; [b]Institute for Biogenesis Research, Department of Anatomy, Physiology, and Biochemistry, University of Hawaii Medical School, Honolulu, HI 96822; and [c]Department of Biology, University of Nevada, Reno, Reno, NV 89557

Contributed by Ryuzo Yanagimachi, December 24, 2014 (sent for review October 23, 2014)

"Pinhead sperm," or "acephalic sperm," a type of human teratozoospermia, refers to the condition in which ejaculate contains mostly sperm flagella without heads. Family clustering and homogeneity of this syndrome suggests a genetic basis, but the causative genes remain largely unknown. Here we report that *Spata6*, an evolutionarily conserved testis-specific gene, encodes a protein required for formation of the segmented columns and the capitulum, two major structures of the sperm connecting piece essential for linking the developing flagellum to the head during late spermiogenesis. Inactivation of *Spata6* in mice leads to acephalic spermatozoa and male sterility. Our proteomic analyses reveal that SPATA6 is involved in myosin-based microfilament transport through interaction with myosin subunits (e.g., MYL6).

flagellum | centriole | infertility | sperm anomaly | microtubule

Male gametes—spermatozoa—are produced in the testis through a process termed spermatogenesis, which can be divided into three phases: mitotic, meiotic, and haploid (1). In the mitotic phase, spermatogonial stem cells proliferate and differentiate into spermatogonia, which subsequently enter the meiotic phase and become spermatocytes. Spermatocytes undergo crossover, followed by two consecutive meiotic cell divisions to produce haploid spermatids. Spermatids then undergo a multistep differentiation process, also called spermiogenesis, to form spermatozoa. Severe disruptions in either the mitotic or the meiotic phase tend to cause azoospermia, whereas spermiogenic defects often lead to reduced sperm counts, aberrant sperm motility, and deformed spermatozoa, a condition termed oligoasthenoteratozoospermia (OAT) in humans (2, 3).

OAT accounts for a significant proportion of male idiopathic infertility cases (2, 4). Numerous cases of acephalic spermatozoa have been reported in teratozoospermic patients (5–19). In these patients, the major anomaly lies in headless spermatozoa in the ejaculate, and the headless spermatozoa were initially called "pinhead sperm" because the investigators mistakenly regarded the retained cytoplasmic droplets, which are usually attached to the midprincipal piece junction of the flagella, as the heads of reduced size (8, 13, 14). Extensive ultrastructral studies on humans and animals with acephalic spermatozoa suggest that this condition results from defects in formation of the connecting piece of spermatozoa during late spermiogenesis, including failure for the proximal centrioles to attach normally to the caudal portion of the sperm nuclei, leading to abnormal head–midpiece alignment, or a nuclear defect that interferes with formation of the implantation fossa, the normal lodging site for the sperm proximal centriole (16). Aberrant formation of the connecting piece leads to independent development of the sperm heads and flagella, and eventually these structures become separated within the seminiferous tubules or during their transition through the seminal tract as a consequence of increased instability of the head–midpiece junction (16, 18).

Several features of the human "acephalic spermatozoa," including its uniform phenotype, origin as a systematic alteration of spermiogenesis, unresponsiveness to hormonal treatment, and familial incidence, suggest a genetic origin of this condition (8, 16, 18–20). Mice lacking *Odf1*, a gene encoding outer dense fiber protein 1, display fragile sperm connecting pieces in addition to a disorganized mitochondrial sheath and defective outer dense fibers (ODFs) (21). Inactivation of *Oaz3*, a gene encoding ornithine decarboxylase antizyme 3, also leads to fragile sperm connecting pieces, despite the observation that all major structures of the connecting piece appear to be intact in mice (22). Neither of the two KO lines displays uniformly 100% acephalic spermatozoa, however, suggesting that in the absence of these genes, the connecting piece still can be formed, but in many spermatozoa it is not strong enough to maintain stability. Moreover, whether the effects represent the primary defects owing to ablation of the genes or secondary to other relevant factors remains unclear. Overall, the genetic causes of homogenous acephalic spermatozoa are largely unknown.

Spata6 is known to be expressed exclusively in the testis with multiple transcript isoforms, and a previous attempt to inactivate *Spata6* was unsuccessful because the chimeras failed to transmit the mutant allele through the germline (23). Here we report that *Spata6* encodes a protein that is highly conserved across all vertebrate species and expressed exclusively in developing spermatids and mature spermatozoa. Ablation of *Spata6* completely disrupts connecting piece formation, leading to acephalic spermatozoa in mice.

Significance

Male infertility due to acephalic spermatozoa has been reported in both animals and humans, but its cause remains largely unknown. Here we report that inactivation of *Spata6*, an evolutionarily conserved gene, in mice leads to failure in development of the connecting piece during late spermiogenesis, along with production of headless spermatozoa in the epididymis and ejaculates. The defects may be ascribed to the disrupted myosin-based microfilament transport mediated by SPATA6 through its interactions with myosin light-chain and heavy-chain subunits. This study not only unveils the process of sperm neck formation at both the ultrastructural and molecular levels, but also provides a genetic basis for the production of acephalic spermatozoa in both humans and animals.

Author contributions: S.Y., R.Y., and W.Y. designed research; S.Y., C.J.S., J.B., H.Z., and B.P.B. performed research; R.Y. contributed new reagents/analytic tools; S.Y., C.J.S., J.B., H.Z., B.P.B., R.Y., and W.Y. analyzed data; and S.Y., R.Y., and W.Y. wrote the paper.

The authors declare no conflict of interest.

Freely available online through the PNAS open access option.

[1]To whom correspondence may be addressed. Email: yana@hawaii.edu or wyan@medicine.nevada.edu.

This article contains supporting information online at www.pnas.org/lookup/suppl/doi:10.1073/pnas.1424648112/-/DCSupplemental.

Results

***Spata6* Encodes a Highly Conserved Protein Expressed Exclusively in the Connecting Piece of Vertebrate Spermatozoa.** Multialignment and phylogenetic analyses of SPATA6 orthologs in 13 vertebrate species revealed that SPATA6 is highly conserved during evolution (*SI Appendix*, Fig. S1). Human SPATA6 shares 88%, 50%, and 33% amino acid sequences with its orthologs in mice, chicken, and zebrafish, respectively. Consistent with a previous study (23), four isoforms of *Spata6* transcripts are predicted in mice (*SI Appendix*, Fig. S2*A*); however, isoform 1 appears to be the sole dominant isoform, with its mRNA and protein detected exclusively in testis among all 10 organs analyzed (*SI Appendix*, Fig. S2*B* and Fig. 1*A*). Both *Spata6* mRNA and protein were detectable in testes at postnatal day (P) 14 (P14), and the levels kept increasing from P21 onward, with the highest levels detected in adult testes (*SI Appendix*, Fig. S2*C* and Fig. 1*B*). This expression pattern suggests that *Spata6* mRNA and protein are expressed in late pachytene spermatocytes and spermatids. Indeed, *Spata6* mRNA were detected only in purified spermatocytes and spermatids (*SI Appendix*, Fig. S2*D*), and in situ hybridization analyses also localized *Spata6* mRNA to spermatocytes and spermatids (*SI Appendix*, Fig. S2 *E* and *F*).

Immunofluorescent staining using rabbit anti-SPATA6 polyclonal antibodies revealed that SPATA6 is localized exclusively to the connecting piece of spermatozoa collected from the epididymis of WT male mice (Fig. 1*C*). Supporting this antibody specificity, the specific staining was completely absent in *Spata6*-null spermatozoa with the head still attached to the flagella (Fig. 1*D*), which accounted for <1% of the epididymal spermatozoa in *Spata6* KO males (see below). Considering the high degree of amino acid similarities among all vertebrates (*SI Appendix*, Fig. S1), we used the same anti-SPATA6 antibodies to stain spermatozoa collected from trouts (Fig. 1*E*), rats (Fig. 1*F*), rabbits (Fig. 1*G*), and monkeys (Fig. 1*H*), as well as ejaculated human spermatozoa (Fig. 1*I*). Specific staining was detected exclusively in the connecting piece of spermatozoa in both fish (Fig. 1*E*) and four mammalian species (Fig. 1 *C*, *D*, *F*–*I*), suggesting that SPATA6 is a structural protein specifically localized to the connecting piece of spermatozoa in vertebrates.

To further determine the subcellular localization of SPATA6, we performed immunogold labeling followed by transmission

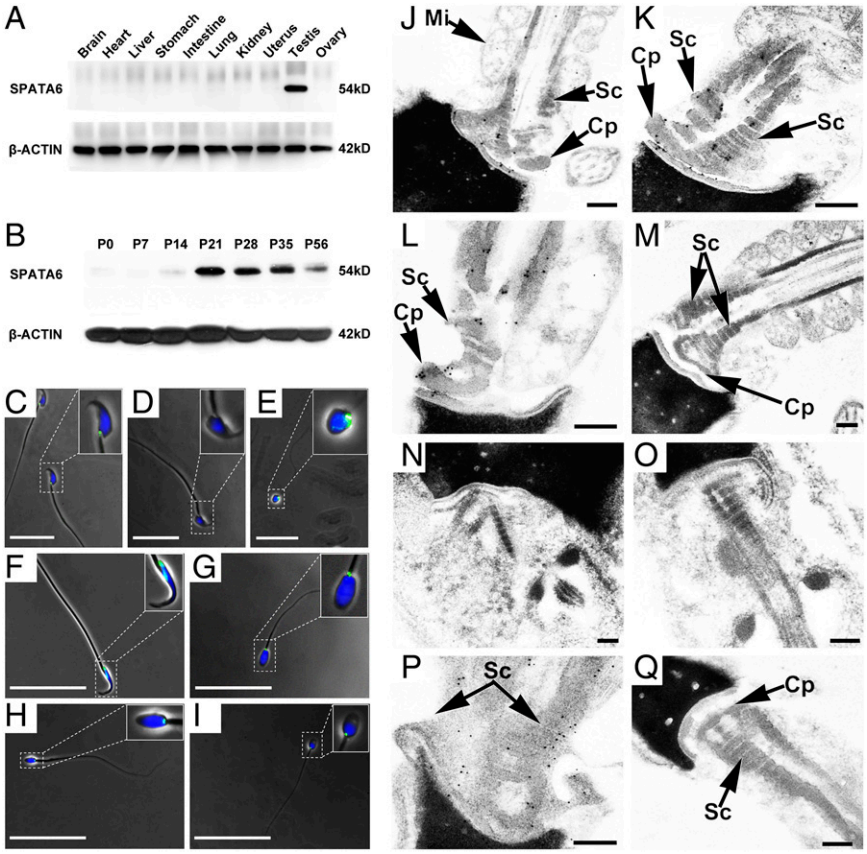

Fig. 1. SPATA6 is localized to the connecting piece of spermatozoa. (*A*) Representative Western blot showing that SPATA6 is exclusively detected in testis. β-ACTIN served as the loading control. (*B*) Representative Western blot showing the onset of SPATA6 expression in P21 testes. β-ACTIN served as the loading control. (*C*–*H*) Immunofluorescent localization of SPATA6 in spermatozoa from six vertebral species, including mouse (*C* and *D*), trout (*E*), rat (*F*), rabbit (*G*), monkey (*H*), and human (*I*). (*Insets*) Digital enlargement of the sperm head-neck mid-piece region framed in the original panels. Note that the specific staining of SPATA6 in green fluorescence is confined to the connecting piece of spermatozoa in all six species analyzed. Intact epididymal spermatozoa collected from *Spata6* KO male mice (*D*), which were extremely rare (<1%), were stained, and no specific signals were detected, demonstrating the specificity of the SPATA6 antibody used. (Scale bars: 25 μm.) (*J*–*Q*) Subcellular localization of SPATA6 in mouse epididymal (*J*–*M*) and rabbit ejaculated (*P* and *Q*) spermatozoa using immunogold staining, followed by TEM. The specific gold particles were confined to the segmented columns and the capitulum of the connecting piece in mouse epididymal (*J*–*L*) and rabbit ejaculated (*P*) spermatozoa, whereas no gold particles were detected in control mouse epididymal (*M*) and rabbit ejaculated (*Q*) spermatozoa, where preimmune serum was used instead of the SPATA6 antibody. As additional controls, step 13–15 elongated spermatids from *Spata6* KO testes were analyzed, and no gold particles were detected in the neck region, which contains no (*N*) or only partially developed (*O*) segmented columns. Sc, segmented column; Cp, capitulum; Mi, mitochondria. (Scale bars: 0.2 μm.)

electron microscopy (IG-TEM) on mouse and rabbit epididymal spermatozoa (Fig. 1 *J*–*Q*). Gold particles were detected mainly in the segmented columns and the capitulum of the connecting piece of spermatozoa from mice (Fig. 1 *J*–*L*) and rabbits (Fig. 1*P*). No specific gold particles were detected in either WT mouse and rabbit spermatozoa stained with preimmune serum (Fig. 1 *M* and *Q*) or *Spata6*-null mouse spermatozoa stained with the SPATA6 antibodies (Fig. 1 *N* and *O*). Taken together, our expression and localization data demonstrate that SPATA6 is an evolutionarily conserved protein localized exclusively to the segmented columns and the capitulum of the connecting piece of spermatozoa.

Inactivation of *Spata6* in Mice Leads to Acephalic Spermatozoa and Male Sterility. To define the physiological role of SPATA6, we generated *Spata6* global KO mice using an embryonic stem (ES) cell line obtained from the Knockout Mouse Project (KOMP) repository (EPD0224_2_B05, ID: CSD33302), in which a "knockout first" gene trap cassette was inserted in between exons 2 and 3 of the *Spata6* locus, leading to a "gene trap" allele (Fig. 2 *A* and *B*). By examining the levels of *Spata6* mRNA (Fig. 2*C*) and protein (Fig. 2*D*) in WT and KO testes, we confirmed that homozygous ($Spata6^{frt/frt}$) mice were completely lacking *Spata6* mRNAs and protein and thus were truly *Spata6*-null. The complete ablation of both *Spata6* mRNA and protein is also

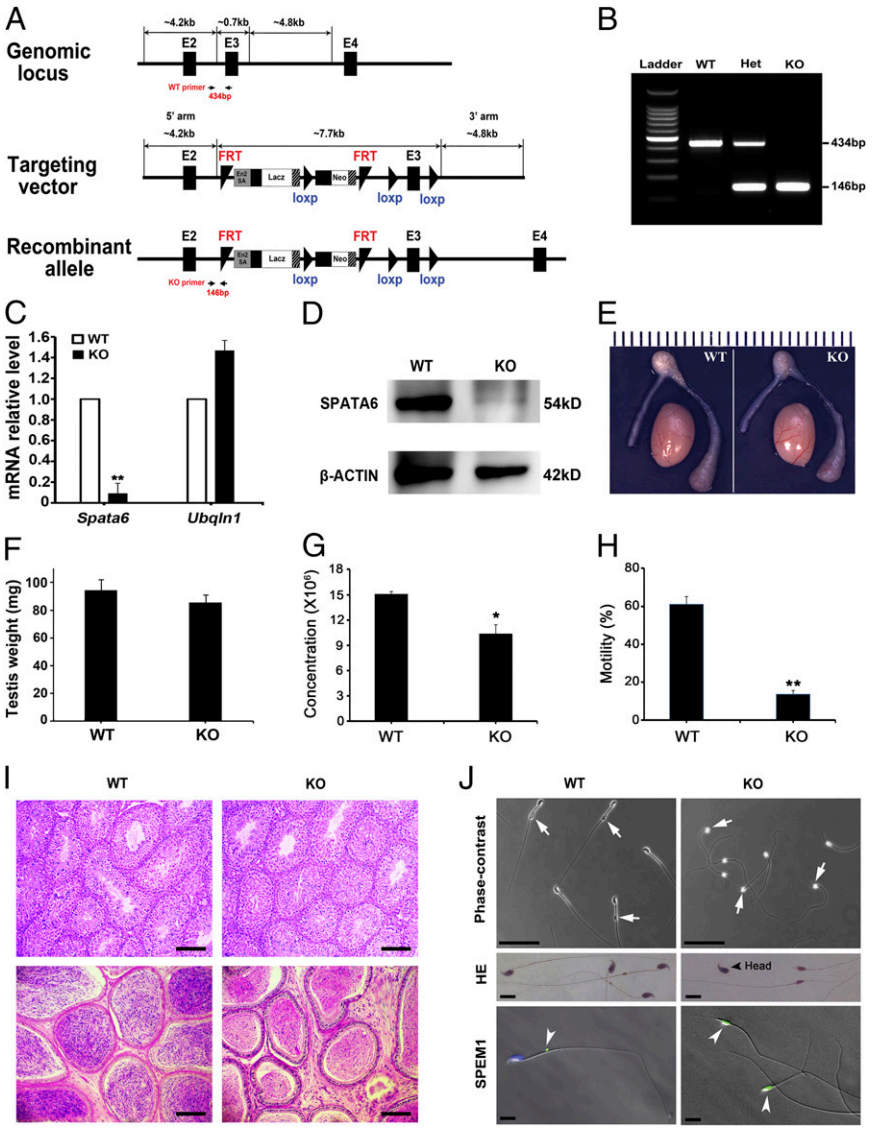

Fig. 2. Inactivation of *Spata6* leads to acephalic spermatozoa and male sterility in mice. (*A*) Schematic illustration of the targeting strategy for generating a *Spata6*-null allele in mouse ES cells. (*B*) Representative result of PCR-based genotyping using tail DNA. (*C*) qPCR analyses of levels of *Spata6* (a testis-specific gene) and *Ubqln1* (a ubiquitous gene) mRNAs in WT and *Spata6* KO testes. *Gapdh* levels were used for normalization. Data are presented as mean ± SEM, $n = 3$. $^{**}P < 0.01$. (*D*) Representative Western blot analysis results showing the detection of SPATA6 protein in WT testes, but not *Spata6* KO testes. β-ACTIN served as a loading control. (*E*) Similar gross morphology of WT and *Spata6* KO testes. (Scale: one unit on the ruler = 1 mm.) (*F*) Similar WT and *Spata6* KO testis weight. Data are presented as mean ± SEM, $n = 6$. (*G*) Significantly reduced epididymal sperm (intact spermatozoa plus sperm flagella) concentration in *Spata6* KO mice compared with WT males. Data are presented as mean ± SEM, $n = 6$. $^{*}P < 0.05$. (*H*) Significantly reduced total motility of *Spata6* KO epididymal headless spermatozoa. Data are presented as mean ± SEM, $n = 6$. $^{**}P < 0.01$. (*I*) Histology of WT (*Left*) and *Spata6* KO (*Right*) testes (*Upper*) and epididymides (*Lower*). (Scale bars: 100 μm.) (*J*) Normal and acephalic spermatozoa in WT (*Left*) and *Spata6* KO (*Right*) epididymides, respectively. Shown are phase-contrast microscopic images (*Upper*; scale bars: 100 μm), hematoxylin and eosin-stained histology (*Middle*; scale bars: 10 μm), and SPEM1 immunofluorescent patterns (*Lower*; scale bars: 10 μm). CDs are indicated by white arrows (*Upper*) or arrowheads (*Lower*). Note that one or two sperm heads occasionally could be seen in the KO epididymis (*Right Middle*, arrowhead).

supported by the data showing an absence of signals in the in situ hybridization (*SI Appendix*, Fig. S2*E*), immunofluorescence (Fig. 1*D*), and IM-TEM (Fig. 1*N*) analyses of the KO testes.

Spata6 KO mice were viable and displayed normal development. Although all of the adult *Spata6* KO females were fertile, the adult male KO mice did not produce any pups after breeding with fertility-proven adult WT female mice for 6 months, suggesting that *Spata6* KO male mice are sterile. To uncover the cause of the male sterility phenotype, we examined the *Spata6* KO males at both gross and histological levels. No differences in testis size and total testis weight were observed between WT and KO mice (Fig. 2 *E* and *F*). Computer-assisted sperm analyses (CASA) revealed reductions in both sperm counts (Fig. 2*G*) and total motility (Fig. 2*H*). Histological examination did not reveal any severe disruptions in the seminiferous epithelia in KO testes (Fig. 2*I* and *SI Appendix*, Fig. S3); however, fewer sperm heads were aligned along the lumen at stage VII in the KO testes compared with the WT stage VII tubules (*SI Appendix*, Fig. S3). Moreover, spermatozoa within the WT epididymis appeared to be more heavily stained with hematoxylin compared with those in the KO epididymis (Fig. 2*I* and *SI Appendix*, Fig. S3). These results suggest the presence of fewer sperm heads in both KO testes and epididymides, and are consistent with the reduced number of sperm heads in both the testicular and epididymal sperm suspensions from the KO mice (see below).

Phase-contrast microscopy examination revealed that the WT epididymal spermatozoa were mostly intact, with the majority carrying the typical cytoplasmic droplets (CDs) (Fig. 2*J, Top* and *Middle Left*), whereas the *Spata6* KO cauda epididymis contained mainly sperm flagella bearing enlarged CD-like structures at the mid-principal piece junction (Fig. 2*J, Top* and *Middle Right*). Through immunostaining of SPEM1, a marker protein for the CD (24), we confirmed that those enlarged cytoplasmic remnants on KO sperm flagella were indeed CDs (Fig. 2*J*, *Bottom*). Quantitative analyses revealed that intact spermatozoa accounted for only ∼7%, ∼4%, and ∼3% of the total sperm cells (intact spermatozoa plus sperm flagella) in the KO testes, KO caput, and caudal epididymides, respectively (*SI Appendix*, Fig. S4). In contrast, the majority (96–99%) of the WT testicular and epididymal spermatozoa were intact (*SI Appendix*, Fig. S4). Moreover, more sperm flagella (93–97%) than sperm heads (14–16%) were present in both KO testes and epididymides compared with the WT samples (*SI Appendix*, Fig. S4). These results suggest that separation of sperm heads from the flagella occurs during spermiogenesis before spermiation, and that the separated sperm heads most likely are engulfed and absorbed by Sertoli cells. Interestingly, ∼10% of the headless sperm flagella collected from the KO cauda epididymis displayed limited progressive motility, and the major waveforms appeared to be confined only to the end piece instead of the principal piece, as seen in WT epididymal spermatozoa (*SI Appendix*, Movies S1 and S2). Taken together, the foregoing findings demonstrate that inactivation of *Spata6* leads to male sterility owing to acephalic spermatozoa with close to 100% penetrance.

Impaired Development of the Connecting Piece in the Absence of SPATA6. The fact that almost all spermatozoa are acephalic and sperm heads are scarce in the KO epididymis suggests that the separation of the sperm head from the flagellum occurs within the seminiferous tubules. To identify the underlying structural defects, we examined the ultrastructure of step 15–16 elongated spermatids in WT and *Spata6* KO testes using TEM (Fig. 3). TEM analyses of the longitudinal sections and cross-sections of WT and KO step 15–16 elongated spermatids revealed no discernable defects in either the nucleus or the acrosome; however, the connecting piece was either completely lacking or only partially developed in *Spata6*-null elongated spermatids (Fig. 3). In WT step 15–16 elongated spermatids, the connecting piece was fully developed and consisted of well-defined segmented columns that united at the anterior and formed the capitulum (Fig. 3*A*). The capitulum was tightly attached to the basal plate of the caudal portion of the nucleus at the implantation fossa. The mitochondria were well aligned to surround the ODFs of the developing mid-piece (Fig. 3*A*). In contrast, normal connecting piece development was never observed in step 15–16 KO elongated spermatids, and two major defects included a complete lack of the segmented columns and/or the capitulum (Fig. 3 *B–D*) and partially formed segmented columns (Fig. 3*E*). In either case, there were no signs of mitochondrial sheath formation (Fig. 3 *B–G*), and a lack of mitochondrial sheath was always associated with misplacement of the annulus, which normally forms a belt at the mid-principal piece junction in step 15–16 WT elongated spermatids and epididymal spermatozoa (Fig. 3 *H* and *I*).

Because of the lack of connecting piece formation, the developing flagella, derived from the distal centrioles, were often misaligned with the developing nuclei/heads (Fig. 3*D*). To determine whether the failure in the assembly of the segmented columns could cause disrupted flagellar development, we further analyzed cross-sections of the *Spata6*-null sperm flagellum. Indeed, we identified severe flagellar defects in *Spata6*-null spermatozoa (Fig. 3*J*). In the mid-piece, WT spermatozoa have a well-defined mitochondrial sheath, enveloping nine ODFs and the axoneme consisting of the typical "9 + 2" microtubules (Fig. 3*J*), whereas the *Spata6*-null spermatozoa displayed a complete lack of or partially formed mitochondrial sheaths, along with incomplete ODFs and axonemes with missing ODFs and axonemal microtubules (Fig. 3*J*). In the end piece, although the fibrous sheath was intact in both WT and *Spata6* KO spermatozoa, disorganized axonemal microtubules were obvious in *Spata6*-null spermatozoa, showing the "8 + 2" or "7 + 2" microtubular compositions instead of the normal "9 + 2" organization in the WT axoneme (Fig. 3*J*). These severe flagellar defects may explain why *Spata6*-null spermatozoa displayed minimal motility (Fig. 2*H* and *SI Appendix*, Movies S1 and S2). Taken together, these ultrastructral analyses reveal that failure of assembly of the segmented columns and the capitulum in developing spermatids represents the primary defects of SPATA6 deficiency, consistent with the exclusive localization of SPATA6 to the segmented columns and the capitulum in the connecting piece of spermatozoa (Fig. 1 *C–Q*).

Normal Development of the Segmented Columns Is Required for Proper Attachment and Alignment of the Sperm Head to the Mid-Piece, As Well As Formation of the Mitochondrial Sheath. Previous ultrastructral studies have documented that flagellar development starts with a functional transformation of the distal centriole into the basal body that serves as the template for the assembly of axonemal doublet microtubules (20, 25). As the flagellar axoneme grows, the basal body migrates to the cell periphery, where distal centrioles dock perpendicularly to the plasma membrane as the axoneme sprouts toward the extracellular space. Meanwhile, the axoneme growth is also accompanied by complex modifications in the dense "pericentriolar materials," from which new proteins or structural components arise and organize to form the nine longitudinal segmented columns of the connecting piece (20, 25). Segmented columns are nine cylindrical structures with periodic densities that fuse cranially to form the capitulum, a curved plate-like disk that links the connecting piece to the basal plate, a dense structure lining the outer nuclear membrane at the implantation fossa (Figs. 1 *J–M* and 3*A*). At the caudal end, each segmented column is continuous with one of the nine ODFs that associate with peripheral microtubular doublets of the growing axoneme (20, 25).

To delineate the developmental process of the connecting piece during late spermiogenesis, we analyzed the ultrastructure of elongating (steps 9–12) and elongated spermatids (steps

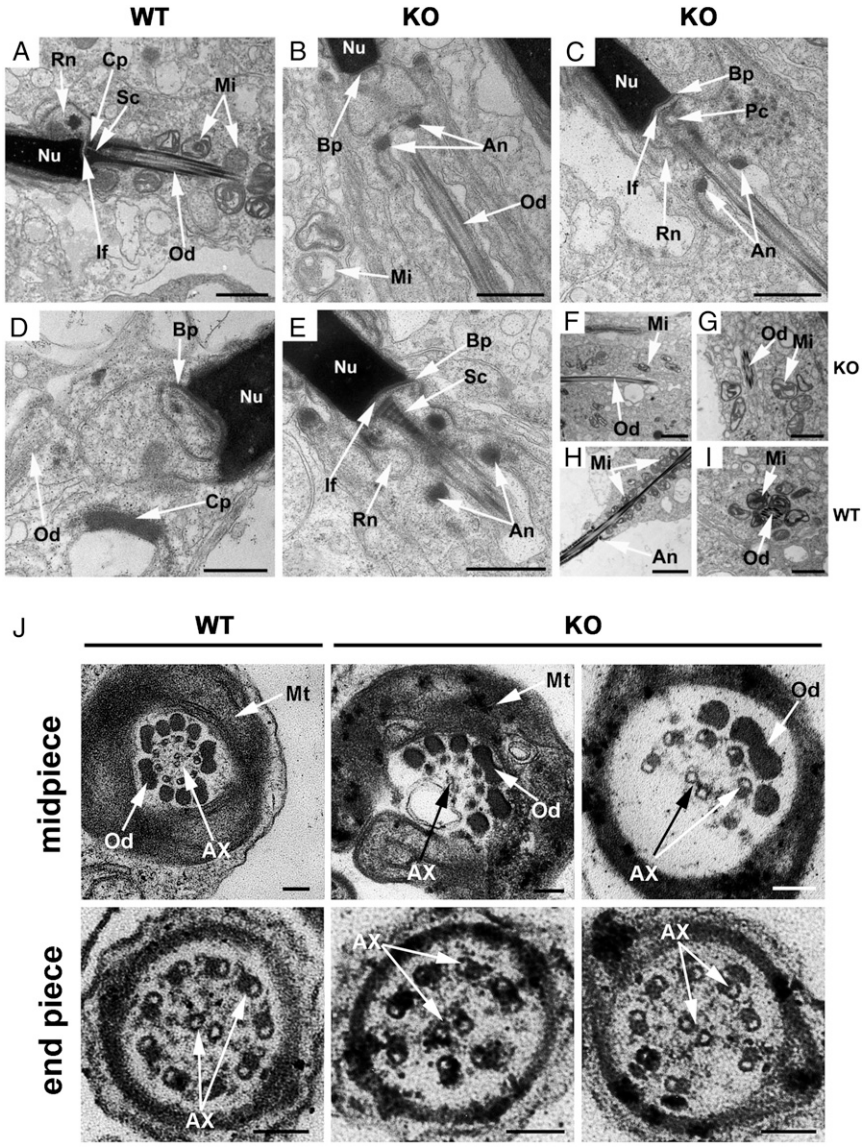

Fig. 3. Impaired development of the connecting piece and the flagellum in *Spata6* KO spermatids revealed by TEM analyses. (*A*) Longitudinal section of a WT step 15 elongated spermatid. The connecting piece consists of the well-defined segmented columns (Sc) and the capitulum (Cp), and the capitulum is attached to the basal plate at the implantation fossa (If). Mitochondria (Mi) are well aligned along the ODFs (Od) in the mid-piece of the flagellum, and the redundant nuclear envelope (Rn) is present. (Scale bar: 1 μm.) (*B*) Longitudinal section of a *Spata6* KO step 15 elongated spermatid. Segmented columns and capitulum are completely absent, although the basal plate (Bp) can be seen. There is a complete lack of mitochondrial sheath along the ODFs, in all cases accompanied by misplacement of the annulus (An). (Scale bar: 1 μm.) (*C*) Longitudinal section of a *Spata6* KO step 16 elongated spermatid. Although the proximal centriole (Pc) is present, the segmented columns, capitulum, and mitochondrial sheath are completely lacking, and the annulus is misplaced. (Scale bar: 1 μm.) (*D*) Longitudinal section of a *Spata6* KO step 15 elongated spermatid. There is no sign of segmented column formation, although a capitulum-like structure can be seen. Moreover, the developing flagellum is misaligned with the developing nucleus (Nu). (Scale bar: 0.5 μm.) (*E*) Longitudinal section of a *Spata6* KO step 16 elongated spermatid. The segmented columns appear to be partial, and there is no obvious capitulum, although the half-baked segmented columns seem to be attached to the basal plate at the implantation fossa. Again, the mitochondrial sheath is completely lacking, and the annulus is misplaced. (Scale bar: 1 μm.) (*F–I*) Longitudinal sections and cross-sections of step 16 spermatids in *Spata6* KO testes showing a lack of formation of the mitochondrial sheath (Mt) and misplacement of the annulus (*F* and *G*) compared with WT step 16 spermatids (*H* and *I*). [Scale bars: 2 μm in longitudinal sections (*F* and *H*) and 1 μm in cross-sections (*G* and *I*).] (*J*) Cross-sections showing the ultrastructure of the mid-piece and the end piece of WT and *Spata6* KO spermatozoa. Note that the mid-piece of KO spermatozoa exhibits structural defects, including malformed (*Upper Middle*) or a complete lack of (*Upper Right*) mitochondrial sheath, partially formed ODFs, and the axonemal microtubules (Ax). In the end piece, WT flagellum consists of fibrous sheath and the typical "9 + 2" arrangement of axonemal microtubules, whereas the KO flagellum contains an atypical "7 + 2" or "8 + 2" composition of axonemal microtubules. (Scale bar: 100 nm.)

13–16), as well as epididymal spermatozoa in WT and KO mice (Fig. 4*A*). In both WT and KO testes, nuclear condensation, nuclear elongation, and flagellar development start in step 9 spermatids. In step 9 spermatids, the proximal centriole was present at the caudal side of the nucleus, and signs of segmented column formation could be seen in the step 10 WT spermatids, but not in the step 10 KO spermatids (Fig. 4*A*). From step 11 to step 12, the segmented columns developed further and became highly defined, and the capitulum started to form in WT spermatids (Fig. 4*A*); however, in KO step 11–12 spermatids, the segmented columns and the capitulum were often absent or only partially formed and severely disorganized (Fig. 4*A*). In step 13–16 WT spermatids, both the segmented columns and capitulum were fully developed, and the flagellum was attached to the basal plates

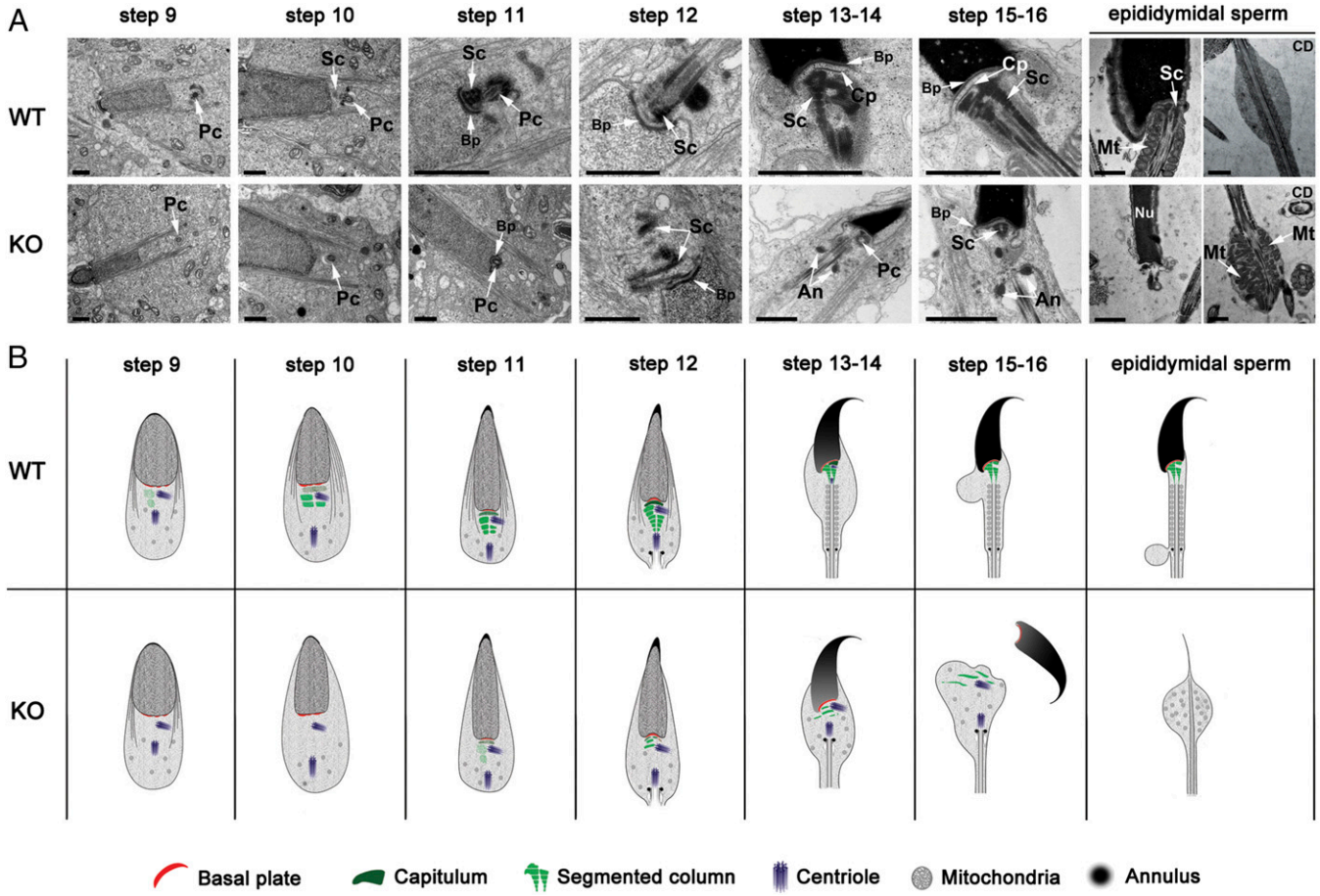

Fig. 4. TEM analyses of the stepwise development of the connecting piece in WT and *Spata6* KO spermatids and epididymal spermatozoa. (*A*) Representative TEM images showing the ultrastructures of step 9–16 spermatids and epididymal spermatozoa in WT and *Spata6* KO mice. In step 9–10 spermatids, the proximal centrioles (Pc) are present at the caudal end of the nucleus (Nu) in both WT and KO spermatids, and signs of segmented column (Sc) formation are occasionally visible in WT spermatids, but not in KO spermatids. In step 11–12 spermatids, the segmented columns are almost fully developed and the capitula (Cp) are visible in WT spermatids; however, in KO step 11–12 spermatids, the segmented columns and capitulum are either completely absent or only partially formed and severely disorganized. In step 13–16 spermatids, both the segmented columns and the capitulum are fully developed, and the flagellum is attached to the basal plates (Bp) at the implantation fossa. In contrast, in KO step 13–16 spermatids, the segmented columns and capitulum are either absent or only partially formed, often accompanied by misalignment of the flagellum and misplacement of the annulus (An). In the WT epididymis, the sperm connecting piece is well developed and tightly connects the sperm flagellum to the sperm head, and the CD is located at the mid-principal junction. In the KO epididymis, sperm heads are rarely seen, and mostly sperm flagella carrying enlarged CDs are present. Interestingly, numerous mitochondria can be seen inside the CDs of KO sperm flagella. (Scale bars: 1 μm.) (*B*) Schematic representation of the stepwise development of the connecting piece in WT and *Spata6* KO mice based on the TEM analyses.

at the implantation fossa (Fig. 4*A*). In contrast, in step 13–16 KO spermatids, the segmented columns and the capitulum were either completely absent or only partially formed, and the annulus was misplaced (Fig. 4*A*). In the KO epididymis, sperm heads accounted for 14–16% of the total sperm cell content (*SI Appendix*, Fig. S4), and the headless sperm flagella usually carried enlarged CDs stuffed with mitochondria (Fig. 4*A*), which were never observed in CDs of WT epididymal spermatozoa (Fig. 4*A*). Taken together, the step-by-step TEM analyses further confirm that in the absence of SPATA6, the segmented columns either do not form or form only partially at a slower pace (Fig. 4*B*), leading to instability in the neck region and, ultimately, complete disconnection between the sperm heads and the flagella within the seminiferous epithelia (Fig. 4*B*).

TEM analyses of the KO sperm heads revealed no discernable defects, suggesting that disruptions in the connecting piece formation may have no impact on sperm head formation. This idea is also supported by the fact that ∼40% of the sperm heads collected from KO cauda epididymides maintained plasma membrane integrity and thus were considered "live" (26, 27), as demonstrated by eosin-nigrosin staining (*SI Appendix*, Fig. S5). To determine whether the KO sperm heads are functionally competent, we evaluated their fertility by intracytoplasmic sperm injection (ICSI). No significant differences in preimplantation development (from two-cell to blastocyst stage) or the number of live-born pups were observed when WT or *Spata6* KO sperm heads were injected into WT eggs (Table 1). Moreover, the *Spata6*$^{+/-}$ offspring derived from ICSI using *Spata6*-null spermatozoa, both male and female, were all healthy and fertile when they reached adulthood. These data suggest that the *Spata6* KO sperm heads, although lacking the connecting piece and separated from the flagella, are fully developed and competent for fertilization and production of normal offspring when injected into WT oocytes.

SPATA6 Interacts with Multiple Myosin Subunits. Because SPATA6 has no known homologs in somatic tissues, it is difficult to predict its molecular function. To gain insight into the molecular action of SPATA6, we adopted an unbiased approach, with immunoprecipitation (IP) followed by liquid chromatography–mass spectrometry (LC-MS), to identify protein partners that interact with SPATA6. Using our rabbit polyclonal anti-SPATA6

Table 1. Development of WT oocytes injected with epididymidal sperm heads from WT and *Spata6*-null males

		Experimental series 1			Experimental series 2			
Sperm genotype	Total oocytes injected, *n* (*n* of experiments)	2PN, *n* (% of 2PN/total)	Two-cell embryos, *n* (% of two-cell embryos/2PN)	Blastocysts, *n* (% of blastocysts/two-cell embryos)	Two-cell embryos transferred, *n* (*n* of experiments)	Recipients, *n*	Live offspring, *n* (%)	Offspring genotype
WT	171 (10)	150 (87.7)	121 (80.7)	61 (50.4)	65 (3)	3	22 (33.9)	$^{+/+}$
Spata6$^{-/-}$	148 (5)	122 (82.4)	110 (90.2)	59 (53.7)	40 (3)	3	14 (35.0)	*Spata6*$^{+/-}$*

*All males developed into fertile adults with normal spermatozoa.

antibodies, we performed IP on both WT and KO testes and then subjected the immunoprecipitants to LC-MS analyses. The IP and LC-MS assays identified a total of 308 putative SPATA6-interacting proteins, all of which showed greater than twofold enrichment (WT vs. KO) and were represented by at least five peptide reads in the LC-MS results (*SI Appendix*, Table S1). Gene Ontology (GO) term analyses identified 29 biological processes that were significantly enriched ($P < 0.05$) among all SPATA6-interacting proteins (*SI Appendix*, Table S2). The three most-enriched biological processes ($P < 0.001$) included cytoskeleton-dependent intracellular transport, actin filament-based process, and actin filament-based movement (Table 2), and the proteins with the greatest fold enrichment were four myosin subunits, including myosin light-chain (MYL) polypeptide 6 (MYL6), myosin heavy-chain (MYH) polypeptide 10 (MYH10), MYL polypeptide 11 (MYH11), and MYH polypeptide 14 (MYH14) (Table 2).

We then chose to analyze MYL6 to validate the proteomic findings. Western blot analyses revealed similar levels of MYL6 expression in both WT and KO testes (Fig. 5*A*), suggesting that *Spata6* inactivation does not affect MYL6 expression. We further performed reciprocal IP assays using antibodies specific for SPATA6 and MYL6. In the immunoprecipitants of SPATA6 antibodies, both SPATA6 and MYL6 were detected in WT testes, but not in KO testes (Fig. 5*B*). In contrast, in the immunoprecipitants of anti-MYL6 antibodies, both SPATA6 and MYL6 were detected in WT testes, whereas MYL6, but not SPATA6, was detected in KO testes (Fig. 5*B*). These results confirm that SPATA6 and MYL6 are indeed bona fide interacting partners in the testes. Further supporting their interactions, our immunofluorescence analyses revealed that both SPATA6 and MYL6 were localized to the manchettes of elongating spermatids (steps 9–12) in WT testes (Fig. 5*C*). Although SPATA6 was eventually confined to the segmented column and the capitulum in spermatozoa (Fig. 1), it was expressed mainly on the manchette in step 9–14 spermatids within the testis (Fig. 5*C*). This finding is common for most, if not all, of the proteins that ultimately become sperm flagellar structural proteins, because the manchette, a microtubule-enriched perinuclear structure present exclusively in step 9–14 spermatids, plays a pivotal role in orchestrating the final assembly of functional spermatozoa, not only by providing the physical forces for shaping the sperm head, but also by serving as a "conveyer belt" that mediates the efficient transportation and processing of proteins required for sperm flagellar assembly (28–33).

Myosin has been considered a molecular motor that converts chemical energy (i.e., ATP) to mechanical power to generate force and to achieve movement in muscle and nonmuscle cells (34). Myosin is composed of two myosin heavy chains, two regulatory light chains, and two essential light chains (35). As a major form of cytoskeleton-dependent intracellular transport, myosin is known to bind actin filaments and to function in the transport of protein cargos in the cytoplasm (36, 37). Interactions between SPATA6 and myosin light and heavy chain subunits strongly suggest that SPATA6 is involved in myosin-based microfilament transport, which may be responsible for transporting basic building blocks for the assembly of the segmented columns during connecting piece formation in developing spermatids (Fig. 5*D*).

Discussion

Spermatozoa in most species adopt a tadpole-like shape, and the sperm head and tail are bridged by the connecting piece, which not only serves as a physical linkage, but also participates in sperm motility by initiating and regulating the waveforms during swimming (38–41). Given the high degree of similarity in sperm shape, it is not surprising that many spermiogenic genes are highly conserved across vertebrate species. In this study, we report that *Spata6*, as one of the highly conserved spermiogenic genes, encodes a protein expressed exclusively in elongating and elongated spermatids, as well as mature spermatozoa, and is essential for proper assembly of the segmented columns and capitulum during the development of the sperm connecting piece.

An earlier attempt to inactivate *Spata6* was unsuccessful owing to failure of germline transmission of the mutant allele (23). The fact that their high-percentage chimeric embryos tend to die suggests that genes other than *Spata6* might have been targeted or affected in that study, because we succeeded in germline transmission of the *Spata6*-null allele, and *Spata6*-null mice are viable and develop normally except for male infertility. The primary defects in KO testes lie in the malformation or total lack of formation of segmented columns in elongating and elongate spermatids, which is consistent with the exclusive localization of

Table 2. GO term analyses of biological processes enriched among SPATA6-interacting proteins

Biological process	Count	Genes	Fold enrichment	*P* value
Cytoskeleton-dependent intracellular transport	4	*Myl6, Uchl1, Myh14, Myh10*	27.00	4.06E-04
Actin filament-based process	6	*Myl6, Myh11, Myh14, Cap1, Calr, Myh10*	7.59	1.06E-03
Actin filament-based movement	3	*Myl6, Myh14, Myh10*	44.55	1.94E-03
Cell redox homeostasis	4	*Prdx6, Prdx4, Pdia4, Prdx1*	14.37	2.57E-03
Cell proliferation	6	*Apoa1, Nasp, Uchl1, Prdx1, Park7, Myh10*	5.41	4.62E-03
Carbohydrate catabolic process	4	*Hexb, Pgam1, Pgam2, Pgk2*	11.00	5.47E-03
Cellular component assembly involved in morphogenesis	3	*Fabp9, Myh11, Myh10*	18.56	1.09E-02

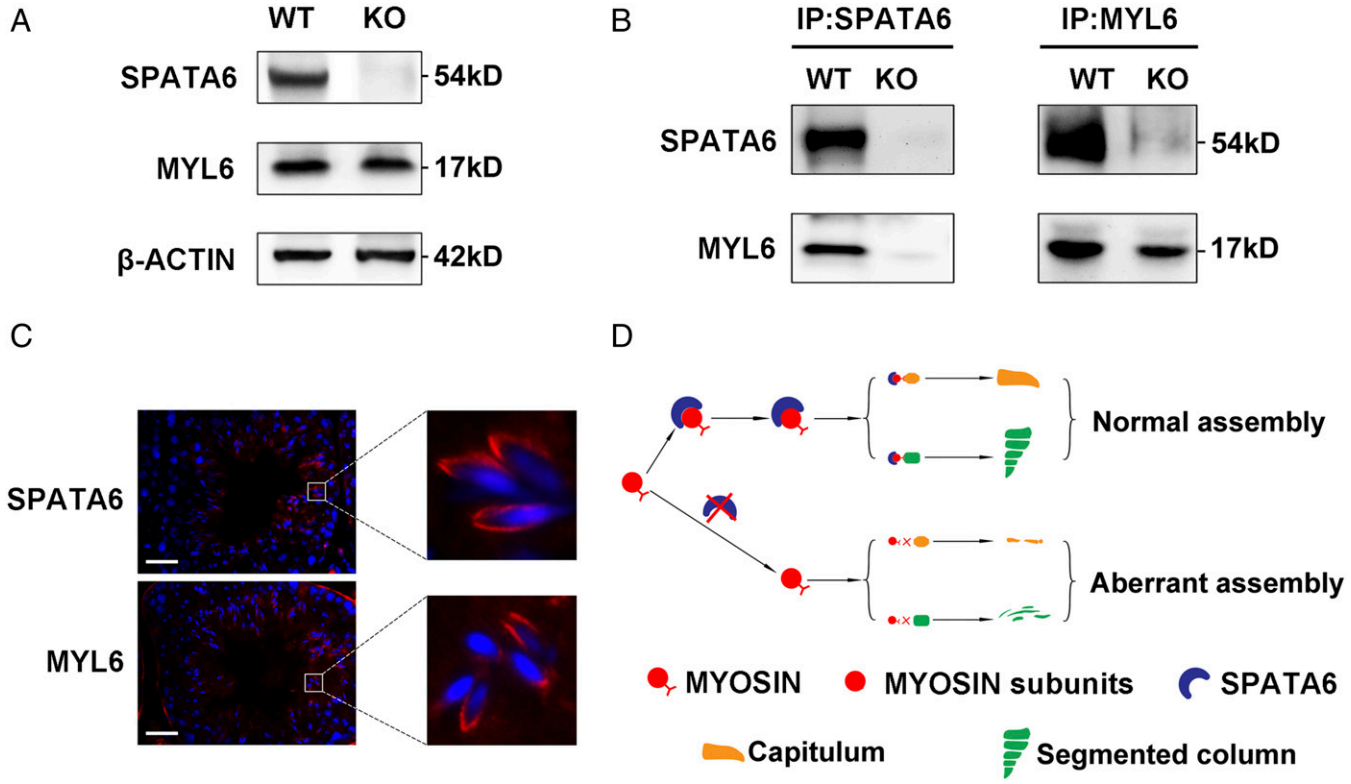

Fig. 5. SPATA6 interacts with myosin subunits during connecting piece formation in elongating and elongated spermatids in mice. (*A*) Representative Western blot results showing the expression of MYL6 in WT and *Spata6* KO testes. β-ACTIN served as a loading control. (*B*) Reciprocal IP assays validating the physical interactions between SPATA6 and MYL6 in WT and *Spata6* KO testes. IP was performed using SPATA6 and MYL6 antibodies, followed by Western blot detection of MYL6 and SPATA6, respectively. (*C*) Immunofluorescence staining of SPATA6 and MYL6 in WT testes. Both proteins are localized to the manchette in elongating spermatids. (Scale bars: 50 μm.) (*D*) Proposed model for the function of SPATA6 in assembly of the sperm connecting piece. Through interaction with myosin subunits (e.g., MYL6), SPATA6 may participate in the myosin-based microfilament transport, which is responsible for delivering and/or organizing the "building blocks" for constructing the segmented columns and the capitulum during connecting piece formation in elongating and elongated spermatids.

SPATA6 to the same structure in the connecting piece of mature spermatozoa. These data suggest that SPATA6 is essential for the proper formation of segmented columns during the development of the connecting piece in mice. Interestingly, similar ultrastructral defects (i.e., malformation or partial formation of segmented columns) have been reported in some human infertility patients with acephalic spermatozoa (16, 18–20, 42), suggesting that a similar underlying mechanism is conserved between mice and humans.

Segmented columns represent a major structure of the connecting piece, and have been suggested to arise from the so-called "pericentriolar materials" (20, 43). Given its exclusive localization to the segmented columns and the capitulum in elongating and elongated spermatids, SPATA6 should represent one of these pericentriolar materials. Considering that the capitulum represents the fused cranial portion of the segmented columns, disruptions in the segmented columns are destined to lead to malformation or absence of the capitulum. Therefore, the primary defects in the absence of SPATA6 involve disruption in segmented column formation or assembly in developing spermatids. Our findings that SPATA6 is involved in myosin-based microfilament transport may explain the failure of segmented column assembly in *Spata6*-null spermatids. One possibility is that assembly of the segmented columns requires transportation of the "building blocks," most likely microtubules, and that this transport function is, at least in part, achieved through the spermatid-specific myosin motor proteins, based on that fact that four types of myosin light- and heavy-chain polypeptides all interact with SPATA6 during assembly of the segmented columns in elongating and elongated spermatids. The absence of SPATA6 may compromise the myosin-based microfilament transport of building blocks for constructing the segmented columns, thereby leading to partial formation or complete lack of segmented columns during development of the connecting piece in elongating and elongated spermatids.

Assembly of the segmented columns is organized by the proximal centrioles, whereas both the flagellar axoneme and ODFs originate from the distal centrioles (20, 25). As such, these two processes appear to be independent of each other, except that the caudal ends of the nine segmented columns in the connecting piece eventually fuse with the nine ODFs in the mid-piece by the time of late flagellar development (20, 25). However, our data strongly suggest that these two processes are in fact interrelated, because when the segmented columns fail to form, or become malformed owing to SPATA6 deficiency, both the axoneme and the ODFs in the mid-piece also become malformed, with aberrant composition of the microtubules and the ODFs, respectively. Given that SPATA6 is expressed exclusively in the segmented columns and the capitulum, the disruptions observed in the axoneme and ODFs most likely represent secondary effects.

The persistence of SPATA6 in mature spermatozoa suggests that SPATA6 is involved in the regulation of myosin motor activity if the associations remain in mature spermatozoa. Alternatively, SPATA6 may interact with other partners in mature sperm and thus exert other unknown functions. Given that the connecting piece is known to initiate and regulate the tail waveforms and overall motility in mature spermatozoa (40, 41, 44, 45), it remains

to be determined whether SPATA6-dependent myosin motor activity contributes to sperm motility. Of note, *Spata6*-null spermatozoa are in fact naturally formed headless sperm flagella, most of which never connect to the sperm head. Interestingly, these headless flagella still display motility, although the waveforms appear to originate from the principal–end piece junction instead of the connecting piece, as is typically observed in WT spermatozoa, suggesting the existence of a second waveform source at the principal–end piece junction that is independent of the first waveform initiated from the connecting piece. This secondary waveform has been reported previously (46), and it will be interesting to use these headless spermatozoa to study the role of the secondary waveform in the overall sperm motility.

Among all reported human cases of acephalic spermatozoa, only several displayed acephalic spermatozoa with full penetrance (~100% headless), with the rest displaying various percentages of acephalic spermatozoa (5–19). Similarly, mice lacking *Odf1* or *Oaz3* also display acephalic spermatozoa with partial penetrance (21, 22). Partial penetrance observed in both humans and animals (5–19, 47, 48) suggests that this condition is variable and can be caused by either a partial loss of function of *Spata6* or mutations in other genes involved in SPATA6-mediated segmented column formation during spermiogenesis. Nevertheless, this study has identified a candidate for screening causative genes for human acephalic sperm conditions.

In summary, we have discovered that SPATA6 is essential for the connecting piece formation during spermiogenesis, and that malfunction of *Spata6* may be involved in human acephalic sperm conditions.

Materials and Methods

Animal Use. The University of Nevada, Reno's Institutional Animal Care and Use Committee approved all animal use protocols. Details are provided in *SI Appendix, Materials and Methods*.

Generation of *Spata6* Mutant Mice. *Spata6* mutant mice were generated using a targeted ES cell clone (EPD0224_2_B05; ID: CSD33302) obtained from the KOMP Repository, in which a "knockout first" gene trap cassette was inserted in between exons 2 and 3 of the *Spata6* gene (Fig. 2*A*). Details are provided in *SI Appendix, Materials and Methods*.

Fertility Test. The fertility test was carried out by mating adult *Spata6* KO (*Spata6*$^{-/-}$) male mice with WT adult female mice with proven fertility for at least 3 mo. A total of eight *Spata6* KO males and eight of their male heterozygous littermates (*Spata6*$^{+/-}$), as the control group, were tested. The number and size of litters sired by each breeding pair were recorded.

Histology and Immunocytochemistry. Histological evaluation was performed on periodic acid-Schiff–stained, paraffin-embedded sections of the testes, and on hematoxylin and eosin-stained epididymal spermatozoa. Details are provided in *SI Appendix, Materials and Methods*.

CASA. Total sperm motility and number were analyzed using the CASA system (version 14.0; Hamilton-Thorne Bioscience). Details are provided in *SI Appendix, Materials and Methods*.

Sperm Head/Flagellum Counting and Eosin-Nigrosin Staining. The total number of intact spermatozoa, sperm heads, and flagella were counted, and the proportions of each of the three types of sperm components were calculated based on the common denominator (i.e., intact spermatozoa plus flagella) (*SI Appendix*, Fig. S4). Details are provided in *SI Appendix, Materials and Methods*.

TEM and IG-TEM. TEM studies were performed as descried previously with minor modifications (24, 49, 50). Details are provided in *SI Appendix, Materials and Methods*.

Real-Time Quantitative PCR Analyses. SYBR Green-based quantitative PCR (qPCR) analyses were performed on an Applied Biosciences 7900HT Real-Time qPCR system. Primers used for the qPCR analyses are listed in *SI Appendix*, Table S3. *Gapdh* served as an internal control. Details are provided in *SI Appendix, Materials and Methods*.

RNA in Situ Hybridization. *Spata6* mRNA in situ hybridization in testis was performed as described previously (51). Details are provided in *SI Appendix, Materials and Methods*.

Western Blot Analyses. A rabbit anti-*SPATA6* antibody (1:1,000) and a rabbit anti-MYL6 antibody (1:500; Abcam catalog no. ab84349) were used for Western blot analyses. Details are provided in *SI Appendix, Materials and Methods*.

IP Followed by LC-MS. SPATA6 IP and LC-MS analyses were conducted as described previously with some modifications (52). Details are provided in *SI Appendix, Materials and Methods*.

ICSI and Embryo Transfer. ICSI was carried out as described previously (53, 54), with slight modifications. Details are provided in *SI Appendix, Materials and Methods*.

Statistical Analysis. Data are reported as mean ± SEM. Statistical differences between datasets were assessed by one-way ANOVA or the *t* test using SPSS 16.0 software. $P \leq 0.05$ was considered to indicate a significant difference and $P \leq 0.01$ to indicate a very significant difference between two groups. ICSI data were analyzed using the χ^2 test compared with the WT group.

ACKNOWLEDGMENTS. This work was supported in part by National Institutes of Health (NIH) Grants HD060858, HD071736, and HD074573 (to W.Y.). The *Spata6* KO mice were generated and maintained in the University of Nevada Genetic Engineering Center supported by NIH Center of Biomedical Research Excellence (COBRE) Grant RR18751. The TEM analyses were made possible by NIH Grants GM103554 and GM103440, which support the COBRE and the IDeA Network of Biomedical Research Excellence. The ES cell clone used for this research project was generated by the trans-NIH Knock-Out Mouse Project (KOMP) and obtained from the KOMP Repository (www.komp.org). NIH grants to Velocigene at Regeneron Inc. (U01HG004085) and the CSD Consortium (U01HG004080) funded the generation of gene-targeted ES cells for 8,500 genes in the KOMP Program, which are archived and distributed by the KOMP Repository at the University of California Davis and Children's Hospital Oakland Research Institute (U42RR024244).

1. Hermo L, Pelletier RM, Cyr DG, Smith CE (2010) Surfing the wave, cycle, life history, and genes/proteins expressed by testicular germ cells, part 1: Background to spermatogenesis, spermatogonia, and spermatocytes. *Microsc Res Tech* 73(4):241–278.
2. Cavallini G (2006) Male idiopathic oligoasthenoteratozoospermia. *Asian J Androl* 8(2):143–157.
3. Yan W (2009) Male infertility caused by spermiogenic defects: Lessons from gene knockouts. *Mol Cell Endocrinol* 306(1-2):24–32.
4. Devroey P (1998) Clinical application of new micromanipulative technologies to treat the male. *Hum Reprod* 13(Suppl 3):112–122.
5. Toyama Y, Iwamoto T, Yajima M, Baba K, Yuasa S (2000) Decapitated and decaudated spermatozoa in man, and pathogenesis based on the ultrastructure. *Int J Androl* 23(2):109–115.
6. Kamal A, et al. (1999) Easily decapitated spermatozoa defect: A possible cause of unexplained infertility. *Hum Reprod* 14(11):2791–2795.
7. Toyama Y, Kazama T, Fuse H, Katayama T (1995) A case of decapitated spermatozoa in an infertile man. *Andrologia* 27(3):165–170.
8. Baccetti B, et al. (1989) Morphogenesis of the decapitated and decaudated sperm defect in two brothers. *Gamete Res* 23(2):181–188.
9. Holstein AF, Schill WB, Breucker H (1986) Dissociated centriole development as a cause of spermatid malformation in man. *J Reprod Fertil* 78(2):719–725.
10. Perotti ME, Giarola A, Gioria M (1981) Ultrastructural study of the decapitated sperm defect in an infertile man. *J Reprod Fertil* 63(2):543–549.
11. Panidis D, et al. (1998) Headless spermatozoa in fertile men. *J Obstet Gynaecol* 18(6): 581–583.
12. Panidis D, et al. (2001) Headless spermatozoa in semen specimens from fertile and subfertile men. *J Reprod Med* 46(11):947–950.
13. Perotti ME, Gioria M (1981) Fine structure and morphogenesis of "headless" human spermatozoa associated with infertility. *Cell Biol Int Rep* 5(2):113.
14. Le Lannou D (1979) [Teratospermia consisting of the absence of the head of the spermatozoa because of a fault in the joint between the head and the neck of the sperm in man (author's transl)]. *J Gynecol Obstet Biol Reprod (Paris)* 8(1): 43–45.
15. Moretti E, et al. (2011) Two cases of sperm immotility: A mosaic of flagellar alterations related to dysplasia of the fibrous sheath and abnormalities of head-neck attachment. *Fertil Steril* 95(5):1787.e19–1787.e23.

16. Chemes HE, Rawe VY (2010) The making of abnormal spermatozoa: Cellular and molecular mechanisms underlying pathological spermiogenesis. *Cell Tissue Res* 341(3): 349–357.
17. Rawe VY, et al. (2002) A pathology of the sperm centriole responsible for defective sperm aster formation, syngamy and cleavage. *Hum Reprod* 17(9):2344–2349.
18. Chemes HE, et al. (1999) Acephalic spermatozoa and abnormal development of the head-neck attachment: A human syndrome of genetic origin. *Hum Reprod* 14(7): 1811–1818.
19. Chemes HE, et al. (1987) Lack of a head in human spermatozoa from sterile patients: A syndrome associated with impaired fertilization. *Fertil Steril* 47(2):310–316.
20. Chemes HE (2012) Sperm centrioles and their dual role in flagellogenesis and cell cycle of the zygote: Structure, function and pathology. *The Centrosome*, ed Schatten H (Humana Press, New York), pp 33–48.
21. Yang K, et al. (2012) The small heat shock protein ODF1/HSPB10 is essential for tight linkage of sperm head to tail and male fertility in mice. *Mol Cell Biol* 32(1):216–225.
22. Tokuhiro K, et al. (2009) OAZ-t/OAZ3 is essential for rigid connection of sperm tails to heads in mouse. *PLoS Genet* 5(11):e1000712.
23. Oh C, et al. (2003) Characterization, expression pattern and chromosomal localization of the spermatogenesis associated 6 gene (*Spata6*). *Mol Hum Reprod* 9(6):321–330.
24. Zheng H, et al. (2007) Lack of Spem1 causes aberrant cytoplasm removal, sperm deformation, and male infertility. *Proc Natl Acad Sci USA* 104(16):6852–6857.
25. Fawcett DW (1981) *The Cell* (Saunders, Philadelphia).
26. Klimowicz-Bodys MD, Batkowski F, Ochrem AS, Savič MA (2012) Comparison of assessment of pigeon sperm viability by contrast-phase microscope (eosin-nigrosin staining) and flow cytometry (SYBR-14/propidium iodide (PI) staining) [evaluation of pigeon sperm viability]. *Theriogenology* 77(3):628–635.
27. Björndahl L, Söderlund I, Kvist U (2003) Evaluation of the one-step eosin-nigrosin staining technique for human sperm vitality assessment. *Hum Reprod* 18(4):813–816.
28. Kierszenbaum AL, Tres LL (2004) The acrosome-acroplaxome-manchette complex and the shaping of the spermatid head. *Arch Histol Cytol* 67(4):271–284.
29. Lehti MS, Kotaja N, Sironen A (2013) KIF3A is essential for sperm tail formation and manchette function. *Mol Cell Endocrinol* 377(1-2):44–55.
30. Bao J, et al. (2011) RANBP17 is localized to the XY body of spermatocytes and interacts with SPEM1 on the manchette of elongating spermatids. *Mol Cell Endocrinol* 333(2):134–142.
31. Hayasaka S, et al. (2008) Intramanchette transport during primate spermiogenesis: Expression of dynein, myosin Va, motor recruiter myosin Va, VIIa-Rab27a/b interacting protein, and Rab27b in the manchette during human and monkey spermiogenesis. *Asian J Androl* 10(4):561–568.
32. Akhmanova A, et al. (2005) The microtubule plus-end-tracking protein CLIP-170 associates with the spermatid manchette and is essential for spermatogenesis. *Genes Dev* 19(20):2501–2515.
33. Kierszenbaum AL, Gil M, Rivkin E, Tres LL (2002) Ran, a GTP-binding protein involved in nucleocytoplasmic transport and microtubule nucleation, relocates from the manchette to the centrosome region during rat spermiogenesis. *Mol Reprod Dev* 63(1):131–140.
34. Cooper GM (2000) *The Cell: A Molecular Approach* (Sinauer Associates, Sunderland, MA), 2nd Ed.
35. Park I, et al. (2011) Myosin regulatory light chains are required to maintain the stability of myosin II and cellular integrity. *Biochem J* 434(1):171–180.
36. Sun X, Kovacs T, Hu YJ, Yang WX (2011) The role of actin and myosin during spermatogenesis. *Mol Biol Rep* 38(6):3993–4001.
37. Ross JL, Ali MY, Warshaw DM (2008) Cargo transport: Molecular motors navigate a complex cytoskeleton. *Curr Opin Cell Biol* 20(1):41–47.
38. Fawcett DW, Phillips DM (1969) The fine structure and development of the neck region of the mammalian spermatozoon. *Anat Rec* 165(2):153–164.
39. Fawcett DW (1975) The mammalian spermatozoon. *Dev Biol* 44(2):394–436.
40. Woolley DM (2010) Flagellar oscillation: A commentary on proposed mechanisms. *Biol Rev Camb Philos Soc* 85(3):453–470.
41. Woolley DM, Carter DA, Tilly GN (2008) Compliance in the neck structures of the guinea pig spermatozoon, as indicated by rapid freezing and electron microscopy. *J Anat* 213(3):336–341.
42. Porcu G, et al. (2003) Pregnancies after ICSI using sperm with abnormal head-tail junction from two brothers: Case report. *Hum Reprod* 18(3):562–567.
43. Schatten H, Sun QY (2009) The functional significance of centrosomes in mammalian meiosis, fertilization, development, nuclear transfer, and stem cell differentiation. *Environ Mol Mutagen* 50(8):620–636.
44. Ounjai P, Kim KD, Lishko PV, Downing KH (2012) Three-dimensional structure of the bovine sperm connecting piece revealed by electron cryotomography. *Biol Reprod* 87(3):73.
45. Sui H, Downing KH (2006) Molecular architecture of axonemal microtubule doublets revealed by cryo-electron tomography. *Nature* 442(7101):475–478.
46. Woolley DM, Vernon GG (2002) Functional state of the axonemal dyneins during flagellar bend propagation. *Biophys J* 83(4):2162–2169.
47. Blom E (1977) A decapitated sperm defect in two sterile Hereford bulls. *Nord Vet Med* 29(3):119–123.
48. Blom E, Birch-Andersen A (1970) Ultrastructure of the "decapitated sperm defect" in Guernsey bulls. *J Reprod Fertil* 23(1):67–72.
49. Yuan S, Zheng H, Zheng Z, Yan W (2013) Proteomic analyses reveal a role of cytoplasmic droplets as an energy source during epididymal sperm maturation. *PLoS ONE* 8(10):e77466.
50. Stratton CJ, Bayguinov Y, Sanders KM, Ward SM (2000) Ultrastructural analysis of the transdifferentiation of smooth muscle to skeletal muscle in the murine esophagus. *Cell Tissue Res* 301(2):283–298.
51. Bao J, Wu J, Schuster AS, Hennig GW, Yan W (2013) Expression profiling reveals developmentally regulated lncRNA repertoire in the mouse male germline. *Biol Reprod* 89(5):107.
52. Bao J, et al. (2012) STK31(TDRD8) is dynamically regulated throughout mouse spermatogenesis and interacts with MIWI protein. *Histochem Cell Biol* 137(3):377–389.
53. Kimura Y, Yanagimachi R (1995) Intracytoplasmic sperm injection in the mouse. *Biol Reprod* 52(4):709–720.
54. Stein P, Schultz RM (2010) ICSI in the mouse. *Methods Enzymol* 476:251–262.